2023 IEEE/ASME International Conference on Advanced Intelligent Mechatronics (AIM)
June 28-30, 2023. Seattle, Washington, USA

Design and Control of PM-biased Bi-stable Latching Actuator for Low-power Micropump

Eun Kyu Kim*, Bo Min Kang*, Hyo Geon Lee, Hyeong Min Yoon,
Jae Hyun Kim, Jae Woo Jung, and Jun Young Yoon

***Abstract*— While the electromagnetic micropump has low-voltage driving characteristic, it requires continuous energy loss in the form of Joule heating during operations, which can be significantly problematic for battery-driven applications. This paper presents a design and control method of an energy-efficient electromagnetic bi-stable actuator for low-power micropump systems in battery-driven and low-power applications such as wearable drug delivery devices. The proposed actuator design achieves the magnetic bi-stability with the PM-biased flux, reducing the required power by providing zero-power passive latching force and by enabling reciprocating motions with only a short pulsatile current excitation. We also present in this paper the energy-efficient pulse control method using a relationship of the coil voltage and the mover velocity in order to achieve robust switching motions with minimized switching energy. The low-voltage low-power characteristic of the proposed actuator and the feasibility of the control method are experimentally validated. The measured minimum voltage and switching energy are 0.43 V and 1.88 mJ, respectively. The flow volume of the fabricated micropump prototype is measured to be 1.94 μl per latching motion.**

I. Introduction

There has been an increasing demand for micropump systems in various applications that require precise control on the injection of working fluid, such as liquid chromatography [1], [2], drug delivery systems [3]–[5], liquid cooling of micro-electronic chips and circuits [6]–[8], and water management in fuel cells [9]–[11]. In addition to the precise fluid control performance, low-voltage and low-power operation is the key requirement especially for the battery-driven application such as wearable drug delivery devices [12], [13]. In order to develop such energy-efficient micropoump systems, various types of actuators have been utilized such as piezoelectric, electro-osmotic, and electromagnetic actuators. The piezo-electric micropump has the advantages energy efficiency and large flow rates. Such type of micropumps however requires high-voltage operations with costly amplifiers [14], [15]. The electro-osmatic actuators can be miniaturized with the absence of moving parts, however such type also requires high voltages to generate a small velocity [16].

The electromagnetic micropumps have potential for the low-voltage operations as studied in a number of prior art as in [17]–[21]. The major challenge for such elctromagnetic micropumps, however, is the continuous energy consumption during the pump operations. In [22] and [23], for instance, the low-voltage driven electromagnetic micro-actuators for wearable drug delivery and lab-on-chip applications are proposed. However, the proposed actuators requires continuous current source in order to maintain the electromagnetic force between the permanent magnet (PM) and the coil. Such continuous current-consuming can degrade the energy-efficiency, and can be significantly problematic especially for the battery-driven applications.

In this paper, we present the design and control method of an electromagnetic bi-stable actuator for low-power micropumps. With the characteristics of the magnetic bi-stability, the proposed actuator requires only a short pulsatile current excitation to generate reciprocating motions, and the latching force is solely provided by a PM-driven force with no current excitation. We also propose an automated pulse control method in this paper so that the proposed actuator can also achieve robust switching motions with minimized switching energy. The remainder of this paper is organized as follow. Section II introduces the design and working principle of the PM-biased latching actuator for the low-power micropump system. Section III discusses the pulse control method for the robust and low-power switching motion. We present the experimental validation of the proposed pulse control method with the PM-biased latching actuator and also the performance of the micropump system in Section IV, followed by the conclusion in Section V.

II. PM-biased Bi-stable Latching Actuator for Low-power Micropump

A. Overall System Configuration

Fig. 1a shows the overall configuration of the low-power micropump system utilizing the electromagnetic PM-biased bi-stable actuator. The fluidic parts consist of i) the check valves to define the flow direction towards the outlet and ii) the elastic tube acting as a fluidic channel and a fluidic chamber, which can be deformed by the moving part of the actuator. Two symmetric lines with the valve-chamber-valve configuration are merged at the inlet and the outlet

*Both authors are equally contributed to this work.

This work was supported in part by the National Research Foundation of Korea (NRF) grant funded by the Korea government (MSIT)(No. 2020R1C1C100801313 and No. 2021R1A4A103212912) and in part by Korea Institute for Advancement of Technology (KIAT) grant funded by the Korea government (MOTIE)(P0012744, The Competency Development Program for Industry Specialist). *(Corresponding author: Jun Young Yoon)*

E K Kim, B M Kang, H G Lee, H M Yoon, J H Kim, J W Jung and J Y Yoon are with the Department of Mechanical Engineering, Yonsei University, Seoul 03722 South Korea. junyoung.yoon@yonsei.ac.kr

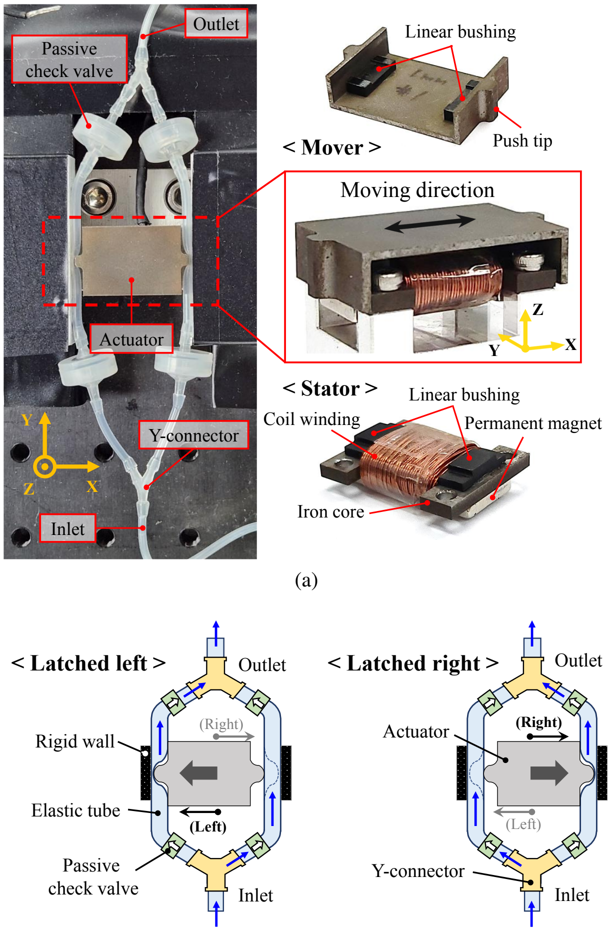

Fig. 1. Low-power micropump system utilizing the electromagnetic bi-stable actuator. (a) Picture of the overall micropump system setup and the actuator parts of the mover and the stator. (b) Schematic of the pumping mechanism as a discrete peristaltic pump where the fluid is intaken in the open-side chamber while discharged in the closed-side chamber as the actuator moves in a reciprocating manner. The flow direction is defined by the passive check valves to pump the fluid from the inlet to the outlet.

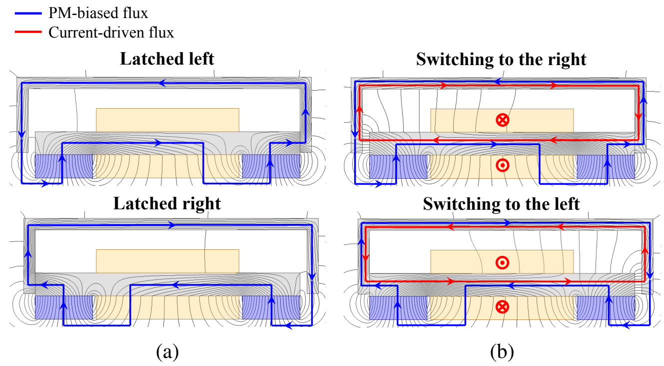

Fig. 2. Working principle of PM-biased latching actuator. (a) The passive latched left and right states are solely achieved by the PM-biased flux without any current excitation on the coil winding. Note that the left and right latched states are defined by the mover position, not by the contacting side. (b) Switching motion by current excitation. When the coil winding is energized, the current-driven flux strengthens the PM-driven flux at one airgap while weakening the other airgap, generating a magnetic force to overcome the latching force to make a switching motion.

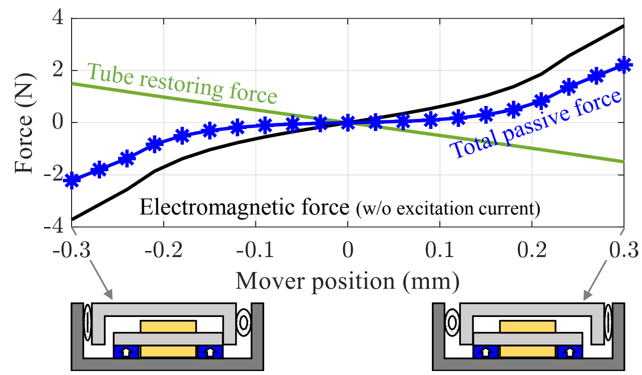

Fig. 3. Passive forces on the mover against the mover position. The ±0.3 mm of the mover position means the right and left latched states. The black curve is the simulated PM-driven reluctance force, applying a maximum of 3.78 N at the end positions to maintain the latched states. The tube restoring force (green curve) tries to restore the deformed tube, acting as the fluid chamber, and yields a maximum magnitude of 1.50 N at the mover end positions. The total passive force of the mover (blue curve) is the sum of the PM-driven reluctance force and the tube restoring force.

using a Y-connection, which is called a double-sided tubing configuration. The actuator consists of the stator as a fixed part and the mover which directly deforms the elastic tubing, acting as a fluidic chamber, by its reciprocating motion. The copper coil (0.3 mm conductor diameter, 140 turns) is wound on the stator iron core, which is made of the soft-magnetic material (SS400). Two N35-grade permanent magnets (PMs) are symmetrically attached below the stator iron core. The mover is also made of SS400 and is placed on top of the stator. A set of linear bushings are installed between the mover and the stator, guiding the mover motion along the X direction. In the integrated actuator, the magnetic flux from the PMs generates the passive attraction force between the mover and the stator, introducing the magnetic bi-stability as presented in depth in Section II-B. Such passive force in the magnetic bi-stable actuator is utilized to maintain the latching state in the micropump system without any current excitation, saving the overall pump operating power and energy. The pumping mechanism is illustrated in Fig. 1b. When the mover in the actuator is latched to close one side of the fluidic chamber discharging the fluid to the outlet, the other chamber becomes open and the fluid is intaken from the inlet, enabling eristaltic pumping operations.

B. Working Principle of PM-biased Latching Actuator

Fig. 2 illustrates the working principle of the PM-biased bi-stable latching actuator. The upward-magnetized PMs are located on both ends of the stator to generate the biased flux, thereby holding the latched states, either to the left or the right, passively without requiring the current excitation as shown in Fig. 2a. Such passive bi-stability is the main characteristic of the proposed actuator to reduce the power consumption. When the current is excited, the current-driven flux is generated on top of the PM-biased flux, strengthening the airgap flux on the

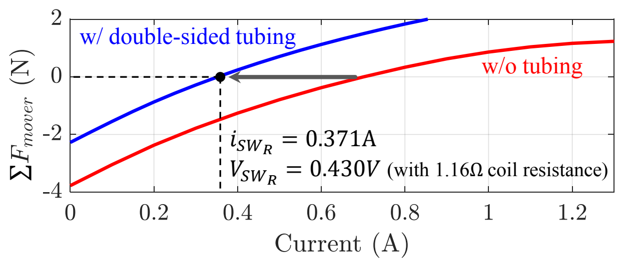

Fig. 4. Simulated actuator force against the current level at the right latched state (+0.3 mm position of the mover). The minimum current required to makes the total F_{mover} positive is the minimum current to overcome the latching force to make a switching motion. Without any tube systems (red curve), a current of at least 0.712 A is required. With a double-sided tube system (blue curve), however, only a current of 0.371 A is required due to the total passive force reduced by the restoring force of the tubing. The corresponding minimum source voltage required is 0.430 V considering the coil resistance of 1.16 Ω.

one side while weakening it on the other side. Such imbalance on the airgap fluxes can generate a magnetic force to overcome the latching force to make a switching motion as depicted in Fig. 2b. Note that we define the minimum current required to make such switching motions as a switching current. As can be seen from the figure, the switching direction can be simply changed by applying the current excitation in the opposite direction.

Fig. 3 shows the passive forces acting on the mover over the mover position in the absence of the current excitation in the pump system. There are two types of passive forces of i) the reluctance force due to the PM-biased flux (black curve) and ii) the restoring force due to elastic properties of the double-sided tubing (green curve). The maximum reluctance force by the PM-biased flux is 3.78 N and the maximum restoring force for the double-sided tubing is 1.50 N. The total passive force on the mover can then be expressed as

$$\sum F_{mover} = F_{EM} + F_s \tag{1}$$

where F_{EM} and F_s indicate the reluctance force and the tubing restoring force, respectively. Since the restoring force acts in the opposite direction to the reluctance force, it reduces the total passive force to be overcome using coil excitation, which leads to the reduced supply voltage, hence saving the switching energy. Note that in the double-sided tubing configuration as shown in Fig. 1, the total passive force acting on the mover becomes 2.28 N. Fig. 4 further shows the advantage of the double-sided tubing restoring force, achieving the lower voltage operation. Without the tube, the current magnitude required to switch the state is 0.712 A while it is reduced by 47 % to 0.371 A with the double-sided tubing. such a lower current level can be generated by a low voltage of 0.43 V considering the coil resistance of 1.16 Ω, manifesting the potential of the proposed actuator in low-voltage and low-power systems, for instance for battery-driven wearable devices.

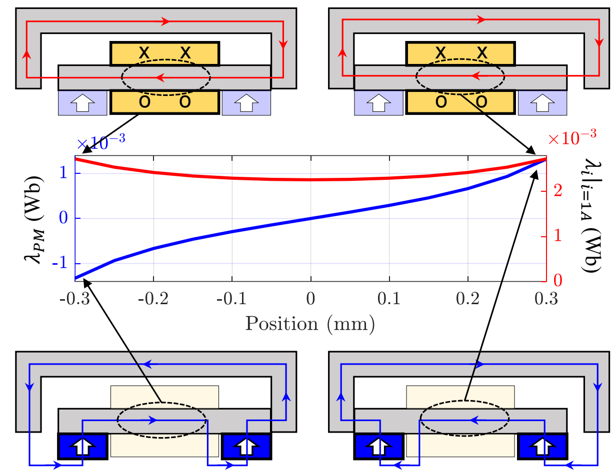

Fig. 5. Simulated PM-biased flux linkage and current-driven flux linkage over the mover position. The blue curve shows the flux linkage by the PM biased flux. As the mover moves from left to right, the direction of the PM-biased flux linked through the coil changes from +X direction to -X direction as illustrated in the dashed circles in the bottom schematic. The red curve shows the flux linkage by the current excitation at 1 A.

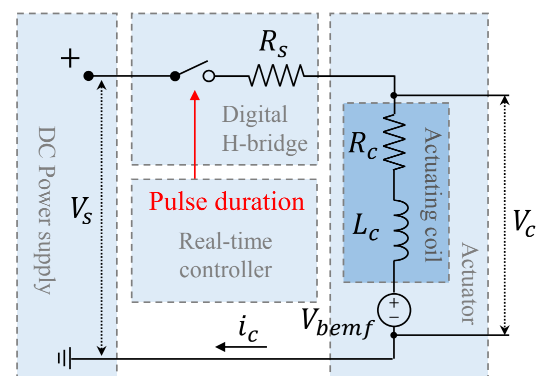

Fig. 6. Circuit diagram to drive the electromagnetic bi-stable actuator, consisting of i) a DC power supply to provide the source voltage V_s, ii) a digital H-bridge with internal resistance of R_s, iii) a real-time controller to monitor the actuating voltage and control the digital H-bridge, and iv) the actuator with its resistance and inductance of R_c and L_c.

III. Pulse Control Method for Low-Power Switching Motion

In this section, we present the energy-efficient pulse control method to detect the latching motion of the bi-stable actuator and therefore to minimize the current excitation duration to achieve the low-power operation of the micropump. The voltage applied to the actuating coil can be expressed as

$$V_c = R_c i_c + \frac{d\lambda}{dt}, \tag{2}$$

where R_c, i_c, and λ represent the resistance of the coil, actuating current, and the flux linkage in the actuating coil. The coil flux linkage λ can be expressed as a superposition of the PM-biased flux linkage λ_{PM} and the current-driven flux linkage λ_i, as shown in Fig. 5. When the mover is at the center position ($x = 0$ mm), the flux generated from both PMs

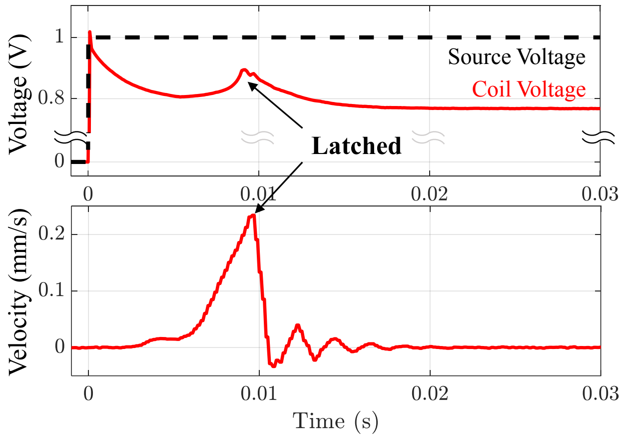

Fig. 7. Measured coil voltage V_c and the mover velocity under the source voltage of $V_s = 1$ V (black dashed curve). The mover position is measured by a laser displacement measurement sensor (LDM) and is used to obtain the mover velocity. The velocity abruptly decreases to zero when latched at $t = 0.0096$ s.

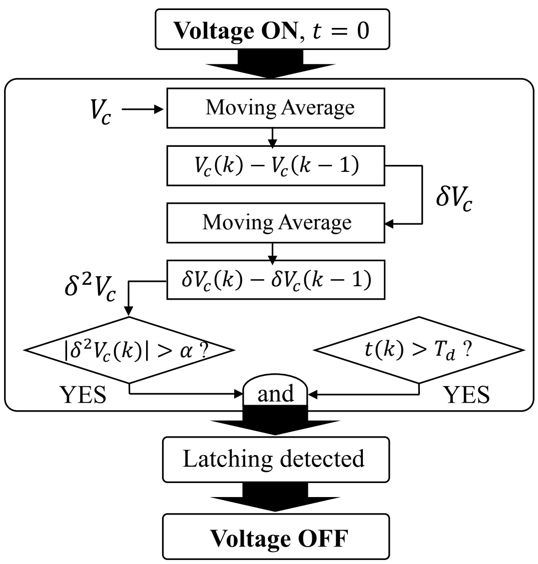

Fig. 8. Flow chart of the proposed pulse control method. The latching is detected when the magnitude of the second derivation of the coil voltage is exceeded a threshold α, and the source voltage is automatically turned off. By setting a dead-zone time T_d, false detection due to the step-input of the source voltage can be prevented.

has the symmetric configuration, thereby resulting in the zero flux linkage in the actuating coil, *i.e.* $\lambda_{PM} = 0$. When the mover is latched to either the left or right side ($x = -0.3$ and 0.3 mm, respectively), on the other hand, the flux path generated from the PMs becomes unsymmetrical, resulting in the net flux linkage λ_{PM} in the $+X$ and $-X$ direction, respectively. The net coil flux linkage from the PMs increases with the mover position x, as shown with the blue curve in Fig. 5. On the other hand, the current-driven flux linkage has relatively less dependency on the mover position, as shown with the red curve in the figure. This is because the total reluctance of the current-driven flux path does not change significantly according to the mover position. The $d\lambda/dt$ term in (2) can then be simplified as

$$\begin{aligned}\frac{d\lambda}{dt} &= \frac{\partial(\lambda_{PM}+\lambda_i)}{\partial i_c}\frac{di_c}{dt} + \frac{\partial(\lambda_{PM}+\lambda_i)}{\partial x}\frac{dx}{dt} \\ &\simeq \frac{\partial \lambda_i}{\partial i_c}\frac{di_c}{dt} + \frac{\partial \lambda_{PM}}{\partial x}\frac{dx}{dt} = L_c\frac{di_c}{dt} + K_v\frac{dx}{dt},\end{aligned} \tag{3}$$

where L_c and K_v represent the inductance of the coil and the back-electromotive-force (back-EMF) constant, respectively. Using (2) and (3), we can track the mover velocity information (dx/dt) by monitoring the coil voltage V_c.

Fig. 6 shows the circuit diagram to drive the electromagnetic bi-stable actuator. A DC power supply (E3631A by Agilent) provides the source voltage V_s, and a custom-made digital H-bridge with its internal resistance of R_s turns on/off the actuating current and regulates its direction. Considering the circuit system shown in the figure, the coil voltage V_c can be expressed as

$$V_c(s) = \frac{L_c s + R_c}{L_c s + R_s + R_c} V_s(s) + \frac{R_s}{L_c s + R_s + R_c} K_v s X(s). \tag{4}$$

The first term in (4) indicates the first-order response of the resistance-inductance (RL) system with respect to the source voltage input V_s. When there is no motion of the mover, *i.e.* $X(s) = 0$, we measure the coil voltage as such RL-response. The second term in (4), on the other hand, involves the back-EMF term generated by the mover motion in the form of a low-pass-filtered velocity. Fig. 7 shows the measured coil voltage and the mover velocity under the step source voltage of $V_s = 1$ V. After the coil excitation at $t = 0$, the mover is accelerated until it reaches the opposite latching position and collides with the stator $t = 0.0096$ s, when the velocity abruptly decreases to zero after a slight oscillatory bounce. As indicated in (4), such rising-and-sharp-drop feature of the velocity during the switching motion is reflected in the measured coil voltage as a local peak at $t = 0.0096$ s as shown in the upper plot of Fig. 7. Therefore, we can detect the latching moment by monitoring such local peak of the measured coil voltage during the switching motions. At the local peak, the second derivative of $V_c(t)$ would have a distinguished magnitude due to the abrupt change in the slope of $V_c(t)$.

Fig. 8 shows the flow chart of the proposed pulse control method utilizing the aforementioned coil voltage relationship with the mover velocity. When the magnitude of the second derivative of the coil voltage $\delta^2 V_c$ exceeds an empirically pre-defined threshold α of 0.0002 V/s^2, the source voltage is automatically turned off. This prevents the redundant current excitation after the switching motion is complete, achieving the robust switching with the minimum energy consumption. Note that moving average filters are applied to reduce the noise effects, and the dead-zone time T_d is defined to prevent the false detection that might be caused by the step input of the source voltage. We discuss the experimental validation of the proposed pulse control method in the following section.

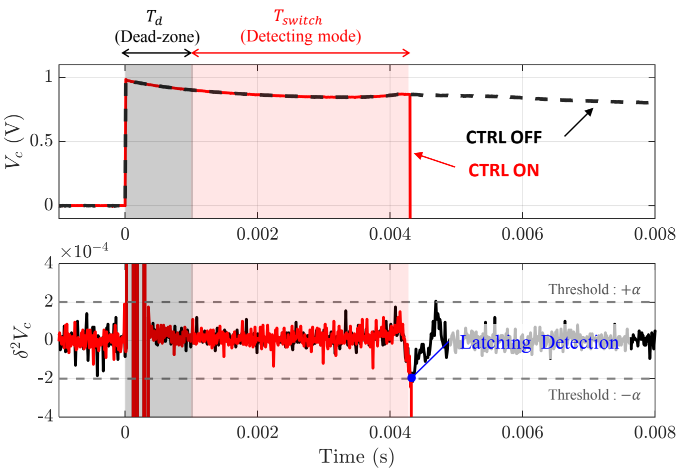

Fig. 9. Measured coil voltage and its second derivative with (red curve) and without (black dashed curve) the pulse time control at $V_s = 1$ V using the double-sided tubing configuration. The dead-zone time $T_d = 1$ ms is applied to prevent false detection on the abrupt voltage fluctuations at the moment of turning on the step source voltage. The moment when the threshold $\alpha = 0.0002$ V/s^2 is exceeded after the dead-zone time is detected as a latching time and the source voltage is turned off.

IV. Experimental Results

A. Pulse Control Test for Low Power Consumption

Fig. 9 shows the measured coil voltage V_c and its second derivative $\delta^2 V_c$ with the proposed pulse control on and off at the source voltage of $V_s = 1$ V. Note that the pulse control method is to detect the local peak point of V_c caused by the sudden velocity change that occurs when the mover reaches the opposite latching position. The red curve in Fig. 9 shows that the source voltage is automatically turned off when the magnitude of $\delta^2 V_c$ exceeds the specific threshold value of $\alpha = 0.0002$ V/s^2 by the real-time monitoring after the dead zone time of $T_d = 1$ ms. The minimum switching energy using the pulse control method is shown in Fig. 10. Note that the minimum source voltage to overcome the passive latching force is measured to be 0.43 V. The switching energy is calculated as

$$E_{sw} = \int_{T_{sw}} V_c(t) i_c(t)\, dt. \tag{5}$$

The minimum switching energy is measured to be 1.88 mJ at the source voltage 0.6 V, validating that the proposed bi-stable actuator requires a significantly low switching voltage and energy.

B. Low-power Peristaltic Pumping Test

Fig. 11 shows the experimentally measured fluid volume and energy consumption of the micropump at $V_s = 1$ V using the pulse control method. The actuator switches every 500 ms, and the flow due to the compression of the tubing is observed each time the actuator latches, either left or right. Every pumping action, the flow volume is measured to be 1.94 μL and the

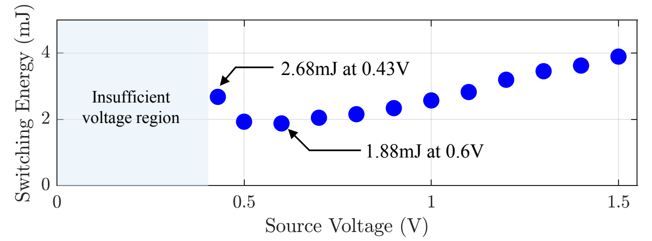

Fig. 10. Measured minimum switching energy using the proposed pulse control according to the source voltage V_s. At the minimum switching voltage of $V_s = 0.43$ V, the minimum required switching energy is measured to be 2.68 mJ. The minimum switching energy of 1.88 mJ is observed at the source voltage of $V_s = 0.6$ V.

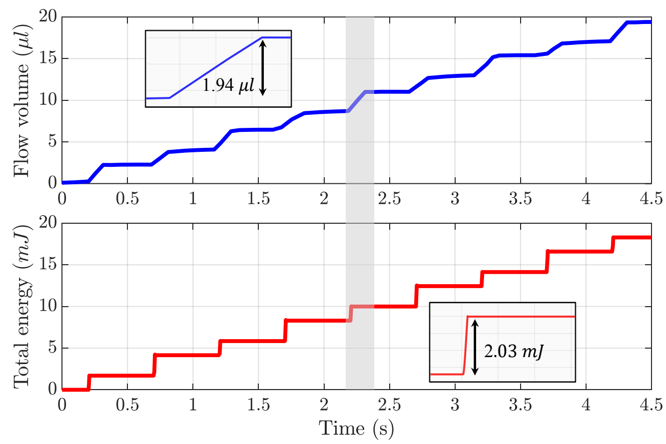

Fig. 11. Measured flow volume and consumed energy of the micropump system. Every pumping action, a flow volume of 1.94 μL is pumped with a minimum switching energy of 2.03 mJ. Note that the switching energy consumes only during the short pulse duration time and the check-valves prevent the reverse flow, yielding discrete peristaltic pumping operations.

switching energy is measured to be 2.03 mJ. As shown in Fig. 11, the flow volume and the energy consumption remain constant between pumping actions. Such low power operating characteristics of the proposed actuator, experimentally demonstrated in this paper, show a great potential to be applied to low-power pumping systems such as wearable devices.

V. Conclusion

This paper proposes the electromagnetic actuator design and energy-efficient pulse control method for a micropump system for low-voltage low-power applications. The required minimum source voltage of the bi-stable latching actuator is measured to be only 0.43 V, achieved by the PM-biased design and also by using the restoring force from the Y-connected double-sided tubing configuration. Utilizing the passive latching force generated by the PM-biased flux, the actuator can maintain the latched states without any additional energy. The latching actuator switches the latching states robustly with the minimized switching energy by the proposed automated pulse control method. The minimum switching energy is measured to be 1.88 mJ at $V_s = 0.6$ V. With a reciprocating motion at a frequency of 1 Hz, every latching motion (0.5 s) generates

1.94μL flow and consumes 2.03 mJ switching energy. The proposed design and control method of the PM-biased bi-stable latching actuator can be readily integrated as a micropump system for the applications requiring low-voltage low-power pumping operations.

REFERENCES

[1] V. Pretorius, B. J. Hopkins, and J. Schieke, "Electro-osmosis: A new concept for high-speed liquid chromatography," *Journal of Chromatography A*, vol. 99, pp. 23–30, 1974.

[2] F. E. Regnier, K. M. Gooding, and S.-H. Chang, "High-speed liquid chromatography of proteins," *Contemporary Topics in Analytical and Clinical Chemistry*, pp. 1–48, 1977.

[3] M. Tan, Y. Xu, Z. Gao, T. Yuan, Q. Liu, R. Yang, B. Zhang, and L. Peng, "Recent advances in intelligent wearable medical devices integrating biosensing and drug delivery," *Advanced Materials*, p. 2108491, 2022.

[4] J. Zhang, J. Xu, J. Lim, J. K. Nolan, H. Lee, and C. H. Lee, "Wearable glucose monitoring and implantable drug delivery systems for diabetes management," *Advanced Healthcare Materials*, vol. 10, no. 17, p. 2100194, 2021.

[5] F. Zhao, X. Chen, J. Zhang, X. Zhang, J. Xie, L. Jin, Z. Liu, J. Zhuang, W. Ren, and Z.-G. Ye, "A wearable, nozzle-diffuser microfluidic pump based on high-performance ferroelectric nanocomposites," *Sensors and Actuators B: Chemical*, vol. 347, p. 130611, 2021.

[6] L. Jiang, J. Mikkelsen, J.-M. Koo, D. Huber, S. Yao, L. Zhang, P. Zhou, J. G. Maveety, R. Prasher, J. G. Santiago, *et al.*, "Closed-loop electroosmotic microchannel cooling system for vlsi circuits," *IEEE Transactions on components and packaging technologies*, vol. 25, no. 3, pp. 347–355, 2002.

[7] V. Singhal, S. V. Garimella, and A. Raman, "Microscale pumping technologies for microchannel cooling systems," *Appl. Mech. Rev.*, vol. 57, no. 3, pp. 191–221, 2004.

[8] S. V. Garimella, V. Singhal, and D. Liu, "On-chip thermal management with microchannel heat sinks and integrated micropumps," *Proceedings of the IEEE*, vol. 94, no. 8, pp. 1534–1548, 2006.

[9] C. R. Buie, J. D. Posner, T. Fabian, S.-W. Cha, D. Kim, F. B. Prinz, J. K. Eaton, and J. G. Santiago, "Water management in proton exchange membrane fuel cells using integrated electroosmotic pumping," *Journal of Power Sources*, vol. 161, no. 1, pp. 191–202, 2006.

[10] N. Islam, "Biased ac electroosmosis micropump for water management in pem fuel cells," in *ASME International Mechanical Engineering Congress and Exposition*, vol. 48715, 2008, pp. 735–738.

[11] S.-C. Yao, X. Tang, C.-C. Hsieh, Y. Alyousef, M. Vladimer, G. K. Fedder, and C. H. Amon, "Micro-electro-mechanical systems (mems)-based micro-scale direct methanol fuel cell development," *Energy*, vol. 31, no. 5, pp. 636–649, 2006.

[12] L. Xu, Y. Yang, Y. Mao, and Z. Li, "Self-powerbility in electrical stimulation drug delivery system," *Advanced Materials Technologies*, vol. 7, no. 2, p. 2100055, 2022.

[13] J. Kim, S. Khan, P. Wu, S. Park, H. Park, C. Yu, and W. Kim, "Self-charging wearables for continuous health monitoring," *Nano Energy*, vol. 79, p. 105419, 2021.

[14] S. Mohith, N. Karanth, and S. Kulkarni, "Performance analysis of valveless micropump with disposable chamber actuated through amplified piezo actuator (apa) for biomedical application," *Mechatronics*, vol. 67, p. 102347, 2020.

[15] H.-K. Ma, W.-F. Luo, and J.-Y. Lin, "Development of a piezoelectric micropump with novel separable design for medical applications," *Sensors and Actuators A: Physical*, vol. 236, pp. 57–66, 2015.

[16] J. P. Urbanski, T. Thorsen, J. A. Levitan, and M. Z. Bazant, "Fast ac electro-osmotic micropumps with nonplanar electrodes," *Applied Physics Letters*, vol. 89, no. 14, p. 143508, 2006.

[17] H. Yu, W. Ye, W. Zhang, Z. Yue, and G. Liu, "Design, fabrication, and characterization of a valveless magnetic travelling-wave micropump," *Journal of micromechanics and microengineering*, vol. 25, no. 6, p. 065019, 2015.

[18] W. Hilber and B. Jakoby, "A magnetic membrane actuator in composite technology utilizing diamagnetic levitation," *IEEE Sensors Journal*, vol. 13, no. 7, pp. 2786–2791, 2013.

[19] V. Tandon, W. S. Kang, T. A. Robbins, A. J. Spencer, E. S. Kim, M. J. McKenna, S. G. Kujawa, J. Fiering, E. E. Pararas, M. J. Mescher, *et al.*, "Microfabricated reciprocating micropump for intracochlear drug delivery with integrated drug/fluid storage and electronically controlled dosing," *Lab on a Chip*, vol. 16, no. 5, pp. 829–846, 2016.

[20] M. Shen, C. Yamahata, and M. Gijs, "A high-performance compact electromagnetic actuator for a pmma ball-valve micropump," *Journal of Micromechanics and Microengineering*, vol. 18, no. 2, p. 025031, 2008.

[21] V. Tandon, W. S. Kang, A. J. Spencer, E. S. Kim, E. E. Pararas, M. J. McKenna, S. G. Kujawa, M. J. Mescher, J. Fiering, W. F. Sewell, *et al.*, "Microfabricated infuse-withdraw micropump component for an integrated inner-ear drug-delivery platform," *Biomedical microdevices*, vol. 17, no. 2, pp. 1–16, 2015.

[22] M. Rusli, P. S. Chee, R. Arsat, K. X. Lau, and P. L. Leow, "Electromagnetic actuation dual-chamber bidirectional flow micropump," *Sensors and Actuators A: Physical*, vol. 282, pp. 17–27, 2018.

[23] R. E. Pawinanto, J. Yunas, A. Alwani, N. Indah, and S. Alva, "Electromagnetic micro-actuator with silicon membrane for fluids pump in drug delivery system," *lab-on a chip*, vol. 1, no. 2, p. 3, 2019.